ISSN : 0974 - 7486 Volume 8 Issue 6

Trade Science Inc.

Materials Science

An Indian Journal

Full Paper

MSAIJ, 8(6), 2012 [251-257]

Hydrothermal synthesis and characterizations of Cd substituted Mn-ferrites

Nasser Y.Mostafa[1,2]*, Z.Heiba[1,3], Omar H.Abd Elkader[4]

[1]Faculty of Science-Taif University, P.O.Box:888 Al-Haweiah, Taif, (SAUDI ARABIA)

[2]Chemistry Department, Faculty of Science, Suez Canal University, Ismailia 41522, (EGYPT)

[3]Physics Department, Faculty of Science, Ain Shams University, Cairo, (EGYPT)

[4]Electron Microscope Unit, Zoology Department, College of Science, King Saud University, Riyadh 11451, (KINGDOM OF SAUDI ARABIA)

E-mail: nmost69@yahoo.com

Received: 18th January, 2012 ; Accepted: 11th February, 2012

ABSTRACT

Well-crystallized Cd-substituted $Mn_{1-x}Cd_xFe_2O_4$ nanoparticles with x having values 0.0, 0.1 and 0.3 have been synthesized by hydrothermal route at 180°C with the help of NaOH as mineralizer. The as-prepared ferrite samples were characterized by XRD, SEM and vibrating sample magnetometer (VSM). The XRD analysis showed that pure single phases of cubic ferrites were obtained with x up to 0.3. However, samples with x>0.3 form sodium cadmium oxide (Na_2CdO_2) beside ferrite phase. The increase in the Cd-substitution up to x=0.3 increased the lattice parameter and the average crystallite size of the prepared ferrites. The saturation magnetization (Ms) increases with increase in Cd-substitution.

KEYWORDS

$MnFe_2O_4$;
Cd-substitution;
Hydrothermal;
Magnetization;
Ferrite;
XRD.

INTRODUCTION

Ferrites are used in many technological applications because of their excellent magnetic and electrical properties. Ferrite spinels (MFe_2O_4, M = Mn, Zn and Ni) are ideal for high-frequency passive components because of its high permeability, resistivity and permittivity. Manganese ferrite ($MnFe_2O_4$) has received a great attention in the areas of magnetic storage devices, microwaves, and electronic devices because it has high magnetic permeability and high electrical resistivity[1-8]. The properties of ferrite materials are determined by their chemical composition, crystallite size and shape, which can be controlled by the preparation and processing parameters. Thus, the interesting features of these materials can be enhanced by controlling the preparation methodology.

Nanoparticles of spinel ferrites display enhanced properties by virtue of their unique electronic structure[9-13]. It was found that when the particle diameter reduced to a definite size, spinel ferrite particles exhibit the so-called superparamagnetic properties, which are of great interest in macroscopic quantum tunneling of spin states[14]. Some of the phenomena like enhanced coercivity, modified saturation magnetization, superparamagnetism, metastable cation distributions,

Full Paper

etc., have been observed in nanoparticles of various ferrites[15-17]. Various methods[18-24] like mechanical milling, inert gas condensation, hydrothermal reaction, oxidative precipitation, sol–gel synthesis and reverse micelle technique are employed for the preparation of ferrites nanoparticles. It was reported that at elevated temperatures (200 - <1000°C), $MnFe_2O_4$ is unstable in air and Mn^{2+} ions on the surface oxidize to form Mn^{3+} ions resulting in the dissociation of the formed $MnFe_2O_4$[25]. So that any preparation method involves calcinations step is not suitable for the preparation of manganese ferrite nanoparticles. On the other hand, ferrites can be prepared via the hydrothermal method at a temperature of about 150-200 °C without the need of high processing temperature or calcinations steps[26]. In recent years, commercial interest in hydrothermal synthesis has been revived in part because a steadily increasing large family of materials, primarily ceramic powders, has emerged that can be prepared under mild hydrothermal conditions[27]. The advantages of hydrothermal synthesis includes, the significant improvement in the chemical activity of the reactant[28, 29]. Easy and precise control of the size, shape distribution, crystallinity of the final product through adjusting the parameters such as reaction temperature, reaction time, solvent type, surfactant type and precursor type[26-29].

Substitution of magnetic and non-magnetic cations in ferrite materials changes thier magnetic and electrical properties[30]. The change in physical and chemical properties of ion substituted spinel ferrites arises from the ability of these compounds to distribute the cations between the available A-sites (tetrahedral) and B-sites (octahedral)[31]. Several cations have been used by many researchers in order to improve the electrical and magnetic properties of manganese ferrites[32-34].

In the present investigation, we synthesized a pure $MnFe_2O_4$ ferrite by the hydrothermal method. Moreover, the effect of Cd ion content on the formation, and magnetic properties of $Mn_{1-x}Cd_xFe_2O_4$ particles (with x varying from 0.1 to 0.3) was also investigated.

MATERIALS AND METHODS

Ferric chloride ($FeCl_3$), manganese chloride ($MnCl_2 \cdot 4H_2O$), cadmium chloride ($CdCl_2.4H_2O$), and sodium hydroxide (NaOH) were of analytical grade reagents. In a typical synthesis process, 80 mmol ferric chloride and 40 mmol manganese chloride and cadmium chloride were mixed, ground uniformly, dissolved in 350 ml distilled water with the assistance of magnetic stirring. The pH was adjusted to 12 with NaOH solution. The volume was completed to 400 ml with distilled water and transferred into a 600 ml Teflon-lined autoclave then heated at 180°C for 20 h. Magnetic stirrer was used within the Teflon-lined autoclave to increase the homogeneity of the produced Cd-substituted ferrite powder. The compositions of the Cd-substituted samples were represented by $Mn_{1-x}Cd_xFe_2O_4$ with x having values 0.0, 0.10, 0.3 and 0.5. The final product was obtained after being washed and filtered several times with distilled water and anhydrous ethanol, then dried at 50 °C in vacuum

X-ray diffraction (XRD) analysis was performed using an automated diffractometer (Philips type: PW1840), at a step size of 0.02°, scanning rate of 2° in 2θ/min., and a 2θ range from 4° to 80°. The values of full width at half-maximum (FWHW) of the peak of the (311) plane was used to calculate the crystallites sizes according to Scherrer's formula.

$$D = K\lambda/[\beta_{1/2}\cos\theta]$$

Where D is the crystallite size in Å, K is Schrrer constant (0.89), Å is the wavelength of X-rays beam (1.5405 Å), □□ is the diffraction angle for the reflection (311) and $\beta_{1/2}$, is defined as the diffraction full width at half-maximum (FWHW), expressed in radians. The FWHW was extracted using X'Pert HighScore Plus program[35]. Determination of the lattice constants were made by least squares refinement of the X-ray diffraction data. Indexing of the powder patterns and least squares fitting of the unit cell parameters was possible using the software X'Pert HighScore Plus[35].

The powders morphology was investigated using SEM (JOEL, Model: JSM-5600, Japan.) equipped with secondary electron detector and EDX. All samples were coated with gold. The magnetic properties of the specimens were measured by a PAR vibrating sample magnetometer at room temperature in a maximum field of 10 kOe.

RESULTS AND DISCUSSION

Figure 1, shows the XRD patterns of Cd-substi-

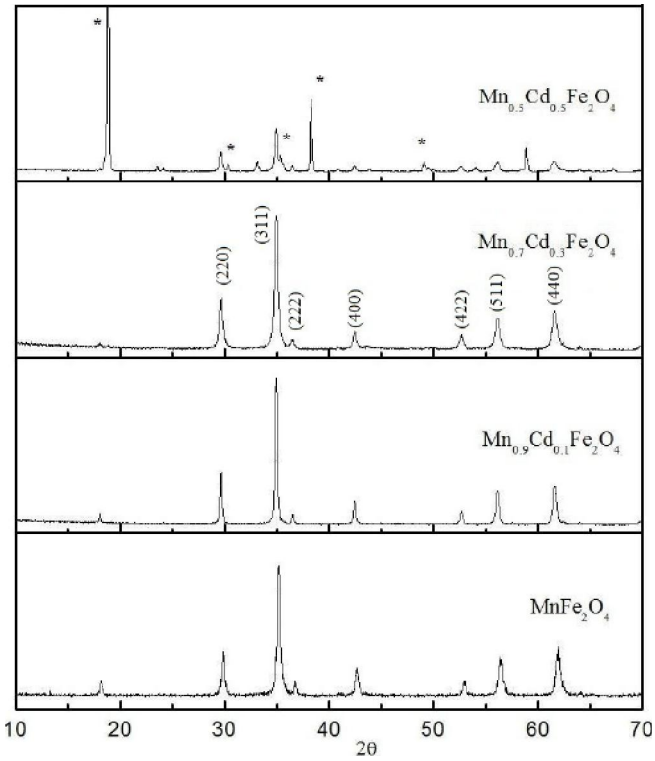

Figure 1 : XRD patterns of $Mn_{1-x}Cd_xFe_2O_4$ synthesized by hydrothermal route (* sodium cadmium oxide (Na_2CdO_2); JCPDS # 00-036-1199).

TABLE 1 : Lattice parameter (a Å) of $Mn_{1-x}Cd_xFe_2O_4$ solid solution.

Sample	x	Lattice constant (a Å)	Crystallite size (nm)
$MnFe_2O_4$	0	8.470	39.8
$Mn_{0.9}Cd_{0.1}Fe_2O_4$	1	8.517	46.7
$Mn_{0.7}Cd_{0.3}Fe_2O_4$	3	8.521	47.5

tuted Mn-ferrite powders prepared by hydrothermal rout. The powder X-ray diffraction analysis ensured the single-phase cubic spinel structure for all values of *x* up to 0.3. The diffraction peaks corresponding to (2 2 0), (3 1 1), (2 2 1), (4 0 0), (4 2 2), (5 1 1) and (4 4 0) planes of $MnFe_2O_4$ were observed (JCPDS # 10-0319). Samples with x =0.5 shows very strong peaks, marked as '*', corresponding to the lines of sodium cadmium oxide (Na_2CdO_2) phase (JCPDS # 00-036-1199) without with very weak peaks of $MnFe_2O_4$. This means that the hydrothermal process resulted in complete conversion of reactants to yield $Mn_{1-x}Ti_xFe_2O_4$ as a single phase with x=0.3 without any calcinations processes. It was reported that manganese ferrite is unstable in air at temperatures 200-1000°C and partially dissociated into α–Fe_2O_3 and Mn_2O_3[25]. Thus, the hydrothermal route is a promising process for the synthesis of a single and pure phase of manganese ferrite. This is an advantage over the other wet chemical routes which need calcinations steps.

The lattice parameter for the cubic $Mn_{1-x}Cd_xFe_2O_4$ spinel powders with 0.0=x=0.3 were calculated. The variation of lattice parameter '*a*' as a function of Cd concentration '*x*' is shown in TABLE 1. The lattice constant increases with increasing cadmium concentration, which can be explained based on the relative ionic radius. The ionic radius (0.78 Å) of Cd^{2+} ions is larger than the ionic radius (0.66 Å) of Mn^{2+} ions. Replacement of larger Cd^{2+} ion for smaller Mn^{2+} ions in the manganese ferrite causes an increase in lattice constant.

TABLE 2 : Ionic radii (Å) of different metal cations in A-sites (tetraheral) and B-sites (Octaheral)[40].

Metal cation	A-sites (tetraheral)	B-sites (Octaheral)
Mn^{2+}	0.66	0.83
Fe^{3+}	0.49	0.55
Cd^{2+}	0.83	0.95

The increase in the values of lattice parameter with low level of Cd-substitutions (x<0.3) can be understood on the basis of average tetrahedral ionic radii of Mn^{2+} ions and Cd^{2+} ions, as summarized in TABLE 2[36]. From Vegard's law, if the radius of displacing ion is larger than the displaced ion, the lattice constant increases. It is well known that the tetravalent Cd^{2+} ions have a strong Tetrahedral (A) sites preference[37]. The octahedral ionic radius of Cd^{2+} ion is 0.61 Å, which is greater than that of Mn^{2+} (0.55 Å), hence the unit cell expands and the lattice constant increases with the increase of Cd^{2+} ions content up to x=0.3.

A clear change was observed in the half peak width of XRD diffractograms, which was reflected in the calculations of the crystallite sizes. TABLE 1, shows the variation of the average crystalline sizes for the cubic spinel phase. It was found that the average crystallite size increased from 39.8 nm for the sample without Cd substitution to 46.7 nm for the sample substituted with x= 0.1. For x=0.3, the crystalline size of the produced ferrite was increased to 47.5 nm. These results are consistent with the results obtained for the lattice parameters, where increasing the lattice parameter may results in increase in the total crystallite sizes. Similar results were reported for other spinel ferrites and PZT

Full Paper

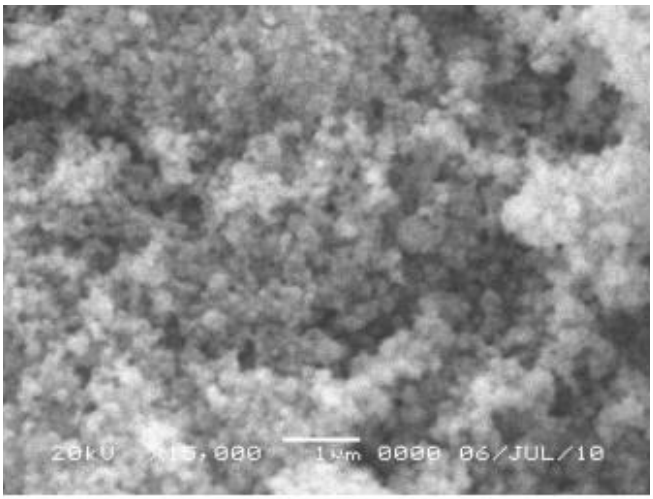

(a)

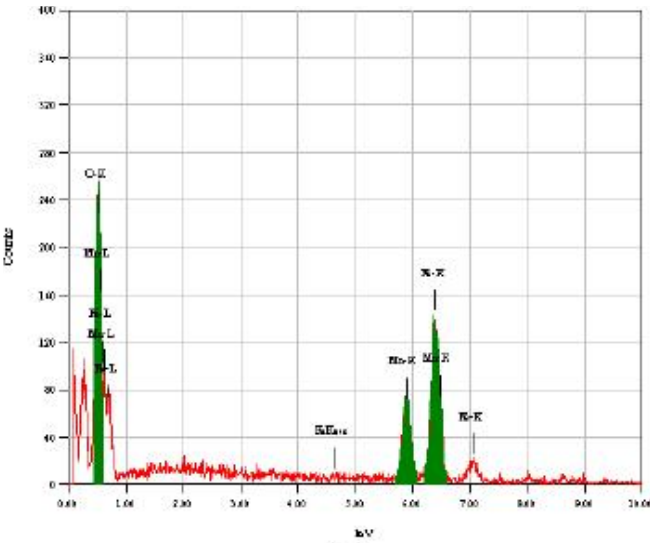

(b)

Figure 2 : SEM micrograph of manganese ferrite ($MnFe_2O_4$) powder prepared by hydrothermal route.

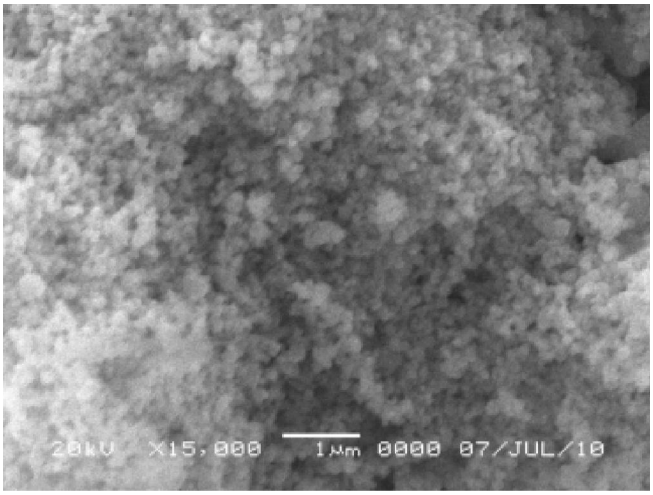

(a)

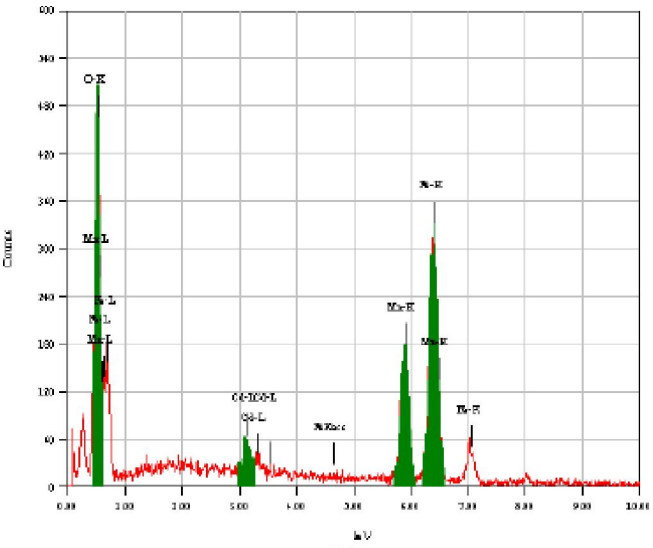

(b)

Figure 3 : SEM micrograph of manganese ferrite ($Mn_{0.9}Cd_{0.1}Fe_2O_4$) powder prepared by hydrothermal route.

ferroelectric materials[38-39].

The microstructures of the as prepared manganese ferrite sample without substitution and with Cd-substitution (up to x=0.3) have been examined by SEM as shown in Figures 2, 3 and 4. It can be observed that the pure ferrite powders (Figure 2 (a)) were quasi-spherical particles with a quite uniform size distribution. Figure 3 (a), shows SEM of Cd-substituted sample (x=0.1). The particles are also spherical with slight bigger grains. These results are consistent with the results of crystallite sizes obtained from XRD data. The chemical compositions of the present ferrite samples after final sintering were determined by energy dispersive X-ray spectroscopy (EDX) and which are also shown in Figures 2, 3 and 4. The EDX spectra of the ferrite samples show the presence of elements (Mn, Cd, Fe and O) without impurities and which indicates the completeness of solid state reaction. Figure 5 shows SEM microstructure of the as prepared manganese ferrite sample with x=0.5. The Figure clearly show the large crystals of cubic sodium cadmium oxide (Na_2CdO_2) phase.

Effects of Cd^{2+} ions substitution on the specific hysteresis loop and saturation magnetization (M_S), of the as prepared $Mn_{1-x}Cd_xFe_2O_4$ with x=0.0 to 0.3 powders were measured at room temperature in a maximum field of 10 kOe. The hysteresis loop are shown in Figure 6. In general, the produced ferrites are soft magnetic material due to the deviation from rectangular form

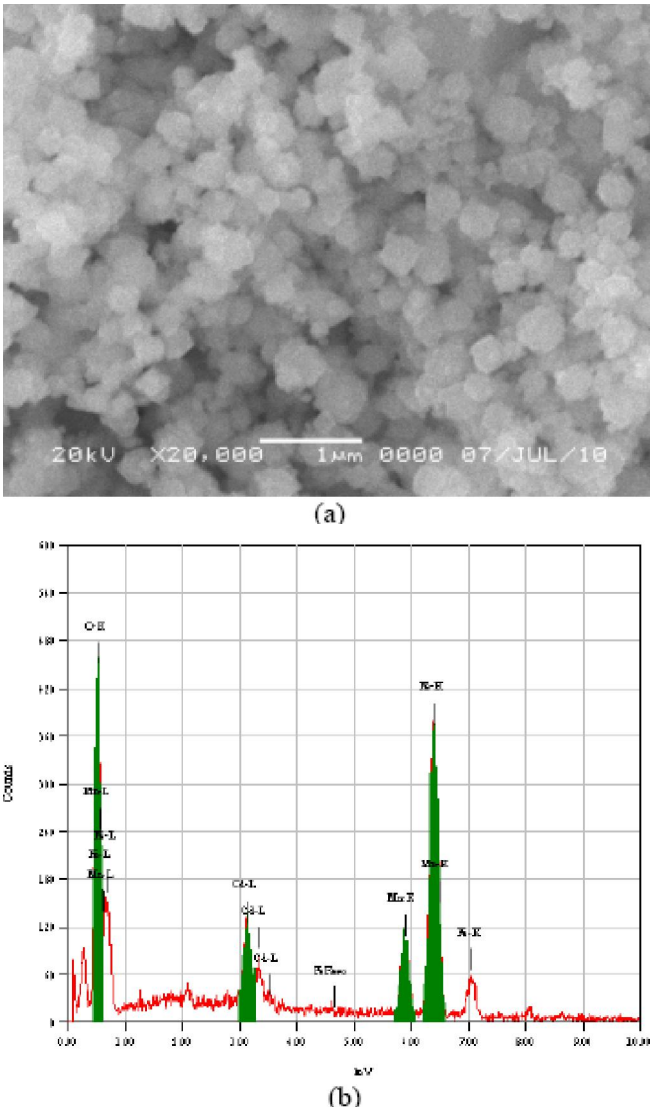

Figure 4 : SEM micrograph of manganese ferrite ($Mn_{0.7}Cd_{0.3}Fe_2O_4$) powder prepared by hydrothermal route.

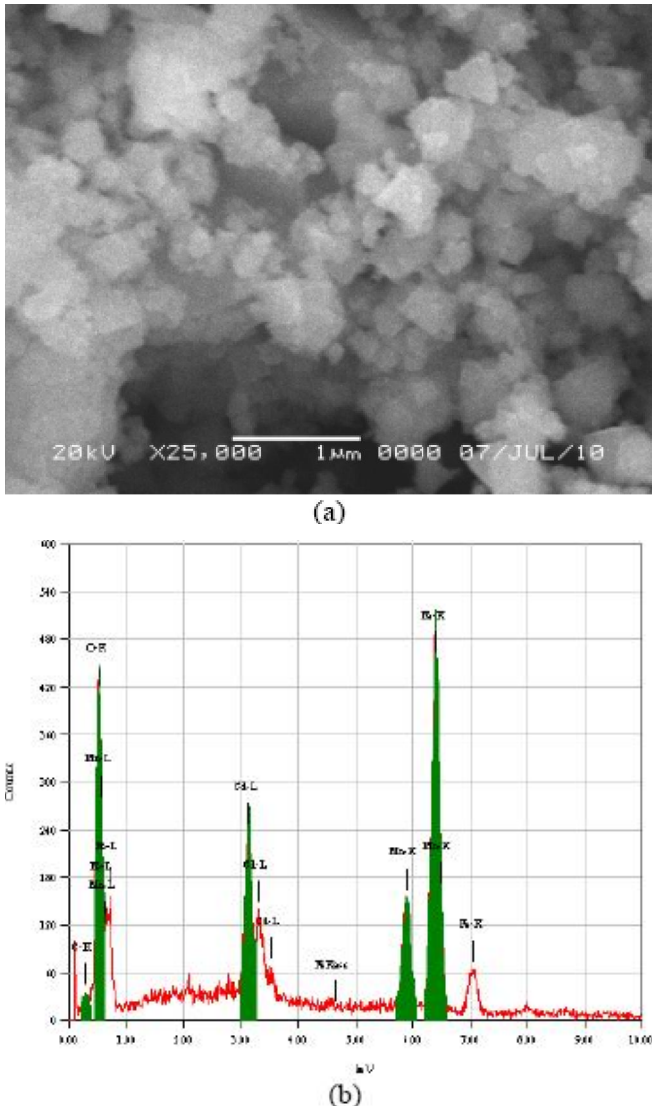

Figure 5 : SEM micrograph of manganese ferrite ($Mn_{0.5}Cd_{0.5}Fe_2O_4$(powder prepared by hydrothermal route.

and their very low coercivity. The M_S of the prepared ferrites is strongly dependent on the Cd^{2+} ion concentration. The M_S of the Cd-substituted Mn-ferrite powders, as shown in Figure 6, increased with the increasing Cd^{2+} ion concentration up to x=0.3. The M_S was increased from 31.08 emu/g for the unsubstituted $MnFe_2O_4$ to 33.88 emu/g for $Mn_{0.9}Cd_{0.1}Fe_2O_4$ particles and slightly increased to 34.46 emu/g for $Mn_{0.7}Cdi_{0.3}Fe_2O_4$ ferrite particles. The magnetization of Cd-substituted $MnFe_2O_4$ can be explained on the basis of Neel's molecular field model and cations distribution between A-sites and B-sites. According to this model, A–B interaction is stronger and more effective than A–A and B–B interactions. The net magnetic moment of the lattice is given by the vector sum of magnetic moments of A and B sublattices $M(x) = M_B(x) - M_A(x)$, where M_B and M_A are the magnetic moment at the octahedral and tetrahedral sites respectively. Generally, $MnFe_2O_4$ prepared by conventional solid state method is known to be 20% inverse spinel[25]. Thus, its structure can be represented by $Mn_{0.8}Fe_{0.2}[Mn_{0.2}Fe_{1.8}]O_4$; where, ions in square bracts occupy B-sites. According to Neel's model discussed above, increasing the occupancy of B-sites with magnetic ions (Fe^{3+} or Mn^{2+}) increases M_S. However, increasing the occupancy of A-sites with magnetic ions decreases M_S.

The increase in saturation magnetization with low level cd-substitution (x =0.1) is due to the substitution of diamagnetic Cd^{2+} ions in the A-sites. Thus Cd-substitution at these low levels does not affect the occu-

Full Paper

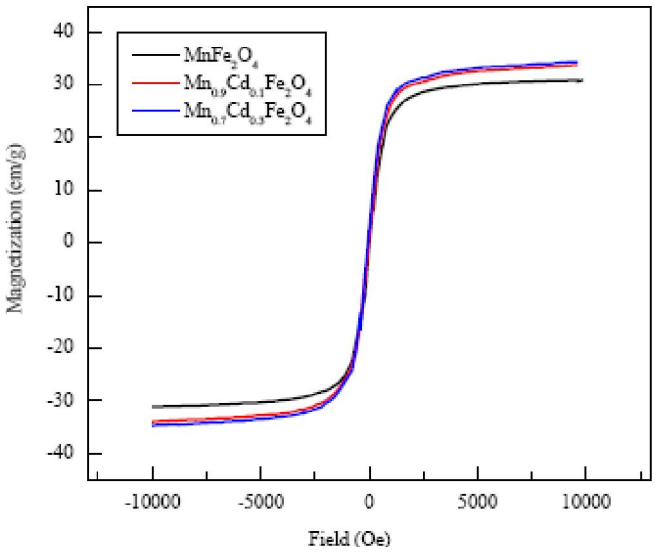

Figure 6 : Effect of Cd ion concentration on the M–H hysteresis loop of $Mn_{1-x}Cd_xFe_2O_4$ powders synthesized by hydrothermal route.

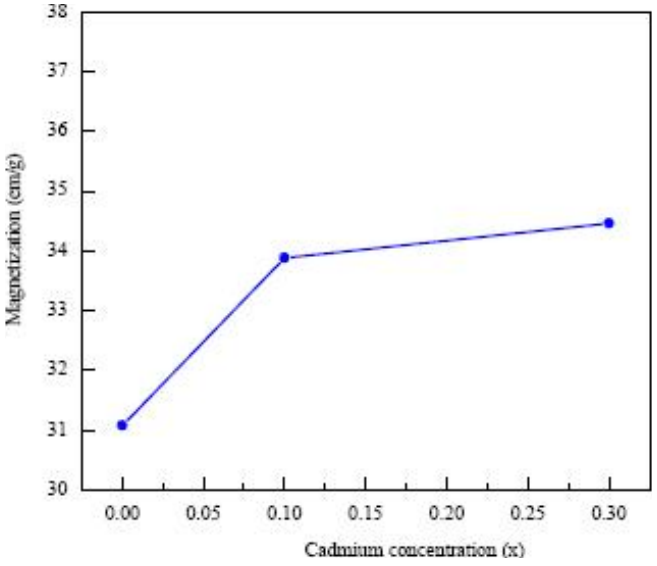

Figure 7 : Effect of Cd ion concentration on the saturation magnetization of $Mn_{1-x}Cd_xFe_2O_4$ powders synthesized by hydrothermal route.

pancy of Fe^{3+} in B-sublattice. However, it decreases the occupancy of Mn^{2+} in A-sublattice, because entering one Thus, the charge compensation mechanism forces Mn^{2+} to expel from the A-sublattice leading to slight overall increase in M_S values.

Figure 7 shows a slight increase in M_S with increasing Cd concentration to $x = 0.3$. For concentrations of x=0.3, the diamagnetic Cd ions occupy both A-sites and B-sites and force Fe^{3+} ions to redistribute in A-sites and cause a slight reduction in the B-sublattice magnetisation.

CONCLUSION

Cd^{2+} ions substitution manganese ferrite particles with diameters ranging from 39 to 47 nm have been synthesized by hydrothermal method at 180°C. At low substitution level (x= 0.1), the Cd^{2+} ions enter the spinel lattice on the tetrahedral A-sites. This leads to an increase in both the lattice parameter and the saturation magnetization. As the substitution level increased to x=0.3, the Cd^{2+} ions start to substitute Mn^{2+} and Fe^{3+} ions in the A-sublattice and B-sublattice, respectavily, which results in lattice parameter increase. However, the saturation magnetization slightly increased due to the dilution of Fe^{3+} in B-sublattice.

ACKNOWLEDGEMENTS

This work was financially supported by a grant from Taif University (Grant No. 1105-432-1).

REFERENCES

[1] M.S.Prasad, B.B.Prasad, B.Rajesh, K.H.Rao, K.V.Ramesh; J.Mag.Mag.Mater., **323**, 2115 **(2011)**.
[2] M.Naeem, N.Abbas Shah, I.H.Gul, A.Maqsood; J.Alloy.Compd., **487**, 739 **(2009)**.
[3] X.Hou, J.Feng, X.Xu, M.Zhang; J.Alloy.Compd., **491**, 258 **(2010)**.
[4] L.Zhen, K.He, C.Y.Xu, W.Z.Shao; J.Magn.Magn. Mater., **320**, 2672 **(2008)**.
[5] Y.W.Ju**,** J.H.Park, H.R.Jung, S.J.Cho, W.J.Lee; Composites Science and Technology, **68**, 1704 **(2008)**.
[6] S.Gubbala, H.Nathani, K.Koizol, R.D.K.Misra; Physica., **B348**, 317 **(2004)**.
[7] M.Popa, P.Bruna, D.Crespo, J.M.C.Moreno; J.Am. Ceram.Soc., **91**, 2488 **(2008)**.
[8] M.N.Ashiq, Na.Bibi, M.A.Malana; J.Alloy.Compd., **490**, 594 **(2010)**.
[9] S.Son, M.Taheri, E.Carpenter, V.G.Harris, M.E.McHenry; J.Appl.Phys., **91**, 7589 **(2002)**.
[10] P.C.Fannin, A.Slawska-Waniewska, P.Didukh, A.Giannitoics, S.W.Charles; Eur.Phys.J.Appl.Phys., **17**, 3 **(2002)**.
[11] T.J.Shinde, A.B.Gadkari, P.N.Vasambekar; J.Mag.Mag.Mater., **322**, 2777 **(2010)**.

[12] A.K.Subramani, K.Kondo, M.Tada, M.Abe, M.Yoshimura, N.Matsushita; J.Mag.Mag.Mater., **321**, 3979 **(2009)**.

[13] I.Safarik, M.Safarikova; Magnetic Nanoparticles and Biosciences. In: H.Hofmann, Z.Rahman, U.Schubert, Editors, Nanostructured Materials, Springer, Wien, 1 **(2002)**.

[14] C.Liu, B.Zhou, A.J.Rondinone, Z.J.Zhang; J.Am.Chem.Soc., **122**, 6263-6267 **(2000)**.

[15] A.S.Albuquerque, J.D.Ardisson, W.A.A.Macedo, M.C.M.Alves; J.Appl.Phys., **87**, 4352 **(2000)**.

[16] I.H.Gul, A.Maqsood, M.Naeem, M.Naeem Ashiq; J.Alloy.Compd., **507**, 201 **(2010)**.

[17] P.C.Fannin, S.W.Charles, J.L.Dormann; J.Magn. Magn.Mater., **201**, 98 **(1999)**.

[18] I.H.Gul, A.Maqsood; J.Alloy.Compd., **465**, 227 **(2008)**.

[19] P.P.Sarangi, S.R.Vadera, M.K.Patra, N.N.Ghosh; Powder Technology, **203**, 348 **(2010)**.

[20] U.Ghazanfar, S.A.Siddiqi, G.Abbas; Materials Science and Engineering, **B118**, 132 **(2005)**.

[21] H.E.Schaefer, H.Kisker, H.Kronmuller, R.Wurschum; Nanostruct.Mater., **1**, 523 **(1992)**.

[22] S.D.Sartale, C.D.Lokhande; Indian J.Eng. Mater. Sci., **7**, 404 **(2000)**.

[23] G.A.El-Shobaky, A.M.Turky, N.Y.Mostafa, S.K.Mohamed; Journal of Alloys and Compounds, **493**, 415-422 **(2010)**.

[24] R.D.K.Misra, S.Gubbala, A.Kale, W.F.Egelhoff Jr.; Mater.Sci.Eng., **B111**, 164 **(2004)**.

[25] E.D.Macklen; J.Inorg.Nucl.Chem., **30**, 2689-2695 **(1968)**.

[26] S.Kumar, R.Kumar, S.K.Sharma, V.R.Reddy, A.Banerjee, Alimuddin; Solid State Commun., **142**, 706 **(2007)**.

[27] W.L.Suchanek, R.E.Riman; Advances in Science and Technology, **45**, 184 **(2006)**.

[28] N.Y.Mostafa, E.A.Kishar, S.A.Abo-El-Enein; J.Alloys.Compd., **473**, 538 **(2009)**.

[29] N.Y.Mostafa, A.A.Shaltout, H.Omar, S.A.Abo-El-Enein; J.Alloys.Compd., **467**, 332 **(2009)**.

[30] C.B.Kolekar, A.Y.Lipare, B.P.Ladganokar, P.N.Vasambekar, A.S.Vaingankar; J.Magn.Magn. Mater., **247**, 142 **(2002)**.

[31] X.Qi, J.Zhou, Z.Yue, Z.Gui, L.Li; J.Magn.Magn. Mater., **251**, 316 **(2002)**.

[32] D.S.Birajdar, D.R.Mane, S.S.More, V.B.Kawade, K.M.Jadhav; Mater.Lett., **59**, 2981 **(2005)**.

[33] L.Nalbandian, A.Delimitis, V.T.Zaspalis, E.A.Deliyanni, D.N.Bakoyannakis, E.N.Peleka; J.Micropor.Mesopor.Mater., **114**, 465 **(2008)**.

[34] M.K.Shobana, S.Sankar, V.Rajendran; Mater. Chem.Phys., **113**, 10 **(2009)**.

[35] HighScore Plus, Full Powder Pattern Analysis Software, V2.2, PANALYTICAL, Almelo, Holland.

[36] CRC Handbook of Chemistry and Physics, 90th Edition, CD-ROM Version **(2010)**.

[37] B.L.Patil, S.R.Sawant, S.A.Patil; Phys.Stat.Solid., **A133**, 147 **(1992)**.

[38] T.K.Kundu, D.Chakravorty; J.Mater.Res., **14**, 3957 **(1999)**.

[39] Z.Xu, X.Dai. J.F.Li, D.Viehland; Appl.Phys.Lett., **68**, 1628 **(1996)**.